Report

Cell Reports

Retino-Cortical Mapping Ratio Predicts Columnar and Salt-and-Pepper Organization in Mammalian Visual Cortex

Graphical Abstract

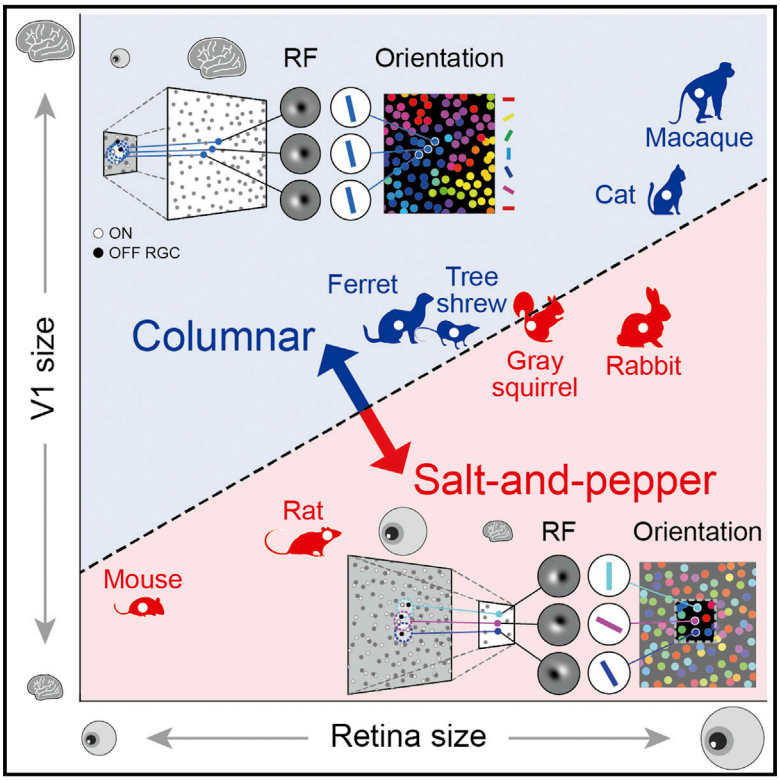

Authors

Jaeson Jang, Min Song, Se-Bum Paik

Correspondence

sbpaik@kaist.ac.kr

In Brief

Across mammalian species, orientation tuning in the primary visual cortex is arranged in different manners, such as columnar orientation map in primates or salt-and-pepper organization in rodents. Here, Jang et al. propose that the retina-to-cortex sampling ratio is the key factor in determining the organization of the orientation tuning.

Highlights

- Determinants of columnar and salt-and-pepper patterns in visual cortex are sought
- Retino-cortical mapping ratio solely predicts cortical patterns across species
- Nyquist sampling model explains sharp parametric division of patterns
- Controlled simulation of retino-cortical sampling ratio reproduces observed patterns

Jang et al., 2020, Cell Reports *30*, 3270–3279
March 10, 2020 © 2020 The Author(s).
https://doi.org/10.1016/j.celrep.2020.02.038

CellPress

OPEN ACCESS
CellPress

Cell Reports
Report

Retino-Cortical Mapping Ratio Predicts Columnar and Salt-and-Pepper Organization in Mammalian Visual Cortex

Jaeson Jang,[1,3] Min Song,[2,3] and Se-Bum Paik[1,2,4,*]
[1]Department of Bio and Brain Engineering, Korea Advanced Institute of Science and Technology, Daejeon 34141, Republic of Korea
[2]Program of Brain and Cognitive Engineering, Korea Advanced Institute of Science and Technology, Daejeon 34141, Republic of Korea
[3]These authors contributed equally
[4]Lead Contact
*Correspondence: sbpaik@kaist.ac.kr
https://doi.org/10.1016/j.celrep.2020.02.038

SUMMARY

In the mammalian primary visual cortex, neural tuning to stimulus orientation is organized in either columnar or salt-and-pepper patterns across species. For decades, this sharp contrast has spawned fundamental questions about the origin of functional architectures in visual cortex. However, it is unknown whether these patterns reflect disparate developmental mechanisms across mammalian taxa or simply originate from variation of biological parameters under a universal development process. In this work, after the analysis of data from eight mammalian species, we show that cortical organization is predictable by a single factor, the retino-cortical mapping ratio. Groups of species with or without columnar clustering are distinguished by the feedforward sampling ratio, and model simulations with controlled mapping conditions reproduce both types of organization. Prediction from the Nyquist theorem explains this parametric division of the patterns with high accuracy. Our results imply that evolutionary variation of physical parameters may induce development of distinct functional circuitry.

INTRODUCTION

Neural tuning to visual stimulus orientation is one of the hallmarks of the primary visual cortex (V1) in mammals. Intriguingly, this tuning in V1 is organized into distinct topographic patterns across species, such as columnar orientation maps in primates (Blasdel and Salama, 1986) and salt-and-pepper type organization in rodents (Ohki et al., 2005) (Figure 1A). From the fact that species of distinct cortical organization are found on separate branches of the mammalian phylogenetic tree, it has been suggested that columnar or salt-and-pepper organization reflect species-specific principles of evolution underlying the development of cortical circuits (Kaschube, 2014; Kaschube et al., 2010).

An alternative view is that cortical development is governed by a universal mechanism, but that disparate architectures can arise from the variation of specific biological parameters, such as the size of V1 (Meng et al., 2012) (Figure 1B, left top), the number of V1 neurons (Weigand et al., 2017), and the range of cortical interaction (Philips et al., 2017). However, further analysis of data for various species revealed counterexamples of this simple prediction, implying that V1 organization may not be simply determined by a single anatomical factor (Van Hooser et al., 2005). In particular, four species of mammals (ferret, tree shrew, rabbit, and gray squirrel) have V1 of comparable size, but it was observed that two of them have columnar orientation maps, while the others have salt-and-pepper organization (Figure 1B, left top). This suggests that the size of V1 may not be a determinant of V1 patterns. Similarly, other candidate parameters, such as visual acuity and body weight, also failed to predict V1 organization of orientation tuning among these four species (Van Hooser et al., 2005) (Figure 1B).

An important clue might be in the observation of the thalamic origin of cortical tuning. Previous studies showed that orientation tuning in V1 is well predicted by the local arrangement of ON and OFF thalamic inputs (Jin et al., 2011; Lien and Scanziani, 2013), implying that functional circuits in V1 might initially be structured by thalamic afferents. In a subsequent study, Mazade and Alonso (2017) also suggested that observed variation of thalamo-cortical projection could play an important role in development of the cortical functions and in maximizing visual acuity. In addition, considering that neurons in the lateral geniculate nucleus (LGN) relay the receptive field of only one to three retinal ganglion cells (RGCs) in most cases (cat: Usrey et al. [1999], monkey: Schein and de Monasterio [1987], mouse: Litvina and Chen [2017]), the structure of the LGN afferents reflects that of the retinal feedforward afferents. Thus, this retinal organization must be taken into account to understand the development of the V1 architecture.

Here, from the analysis of data for eight mammalian species, we propose that the retino-cortical feedforward mapping ratio can solely predict cortical organization of each species. In the following model simulations, we confirm that distinct cortical circuits can arise from different V1 and RGC mosaic sizes. Furthermore, we show that the Nyquist sampling theorem explains this parametric division of cortical organization with high accuracy. Our results suggest that both columnar and salt-and-pepper organization in V1 develop universally with retinal origin (Ringach, 2007), but may bifurcate due to variation of the feedforward circuit.

This is an open access article under the CC BY license (http://creativecommons.org/licenses/by/4.0/).

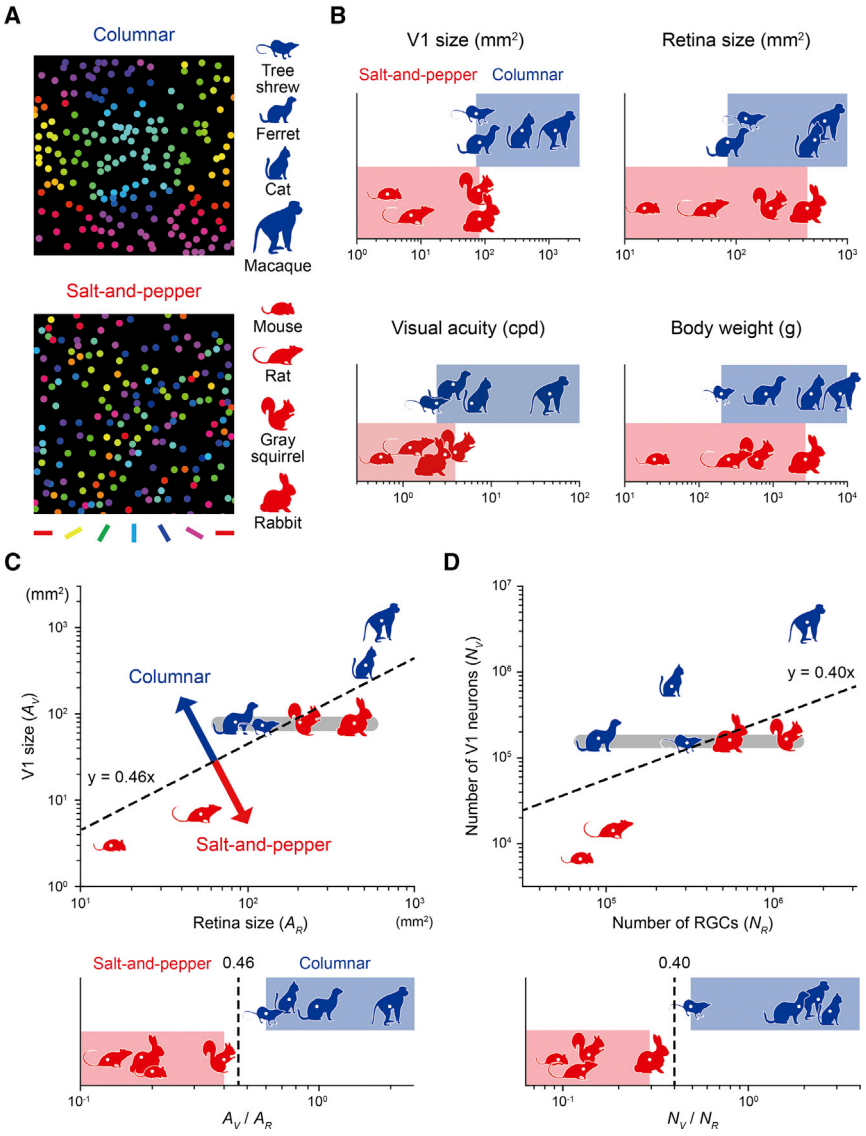

Figure 1. Parametric Division of Spatial Organization of Orientation Tuning across Species

(A) Columnar and salt-and-pepper organization of orientation tuning observed in mammalian species.

(B) Whether a species has columnar or salt-and-pepper organization cannot be clearly predicted by V1 size, retina size, visual acuity, or body weight.

(C) Top: V1 organization of eight mammalian species can be divided by a linear classifier ($y = 0.46x$) in 2D space as a function of V1 and retina sizes. Bottom: V1 organization of each species is well predicted by the ratio between the size of V1 and of a retina.

(D) Similar analysis as in (C) with the number of RGCs and V1 neurons as determinant parameters ($y = 0.40x$).

RESULTS

Parametric Division between Columnar and Salt-and-Pepper Organization in Visual Cortex

We first found that the V1 organization of the eight species reported so far can be successfully divided into columnar maps or salt-and-pepper organization in linear classification, by considering the size of retina (A_R) and the size of V1 (A_V) together (Figure 1C, top; Table 1). In particular, among four species (ferret, tree shrew, rabbit, and gray squirrel; gray shaded area in Figure 1C) that have V1 of comparable size (~80 mm^2), two species (rabbit and gray squirrel) with salt-and-pepper organization have larger retinas than do the others, which have columnar maps (ferret and tree shrew; Figure 1B, right top). Overall, the ratio between the size of V1 and of a retina (A_V/A_R) appears higher for those with columnar maps and solely predicts the V1 organization in all the test data (Figure 1C, bottom). Species having V1 of comparable size, in particular, were successfully divided according to their V1 organization, which could not be predicted by any single biological parameter in previous studies. Next, to examine the mapping between two areas in terms of neuronal units, we tested a prediction based on the ratio between the number of RGCs (N_R) and V1 neurons (N_V) and found that this retino-cortical mapping ratio (N_V/N_R) also successfully predicts the V1 organization of all these species (Figure 1D).

Classification of V1 Organization by Retino-Cortical Mapping Ratio

What, then, is the underlying principle that explains this classification of V1 organization by retino-cortical mapping? Based on previous experimental observations that the orientation tuning in V1 can be predicted by the arrangement of ON and OFF feedforward afferents (Kremkow et al., 2016; Lee et al., 2016), we hypothesized that cortical orientation tuning originates from the spatial arrangement of ON and OFF RGC mosaics (Paik and Ringach, 2011, 2012), and columnar or salt-and-pepper organization in V1 can simply arise due to a different feedforward mapping ratio between RGC and V1 neurons ($\Phi = N_V/N_R$ = number of V1 neurons per RGC), which determines similarity of the cortical tuning in neighboring V1 neurons (Figures 2A–2C).

Using observed RGC mosaics data in cats (Zhan and Troy, 2000), we simulated three scenarios for different sizes of the RGC mosaics and V1. In the model, it was assumed that the entire retinal area is matched to the whole V1 patch, and each V1 neuron receives feedforward inputs from the same size of local ON and OFF RGCs in the area of the corresponding retinal location (see STAR Methods for details). Then, the orientation tuning of each V1 neuron was calculated from the receptive field

Table 1. Experimental Data on the Retina and V1 Anatomy in Diverse Species

	Macaque	Cat	Ferret	Tree Shrew	Rabbit	Gray Squirrel	Rat	Mouse
(A) V1 size (mm^2)	1,257 (Adams et al., 2007; Van Hooser et al., 2005)	380 (Tusa et al., 1978)	83 (Law et al., 1988)	73 (Keil et al., 2012; Sesma et al., 1984)	80 (Hughes, 1971)	82 (Van Hooser et al., 2005)	7 (Espinoza and Thomas, 1983)	3 (Garrett et al., 2014)
(B) Retina size (mm^2)	636 (Kong et al., 2010)	510 (Hughes, 1975)	84 (Henderson, 1985)	122 (Engelmann and Peichl, 1996)	436 (Oyster et al., 1981; Ross and Kay, 2004)	205 (Ross and Kay, 2004)	52 (Hughes, 1979)	15 (Dräger and Olsen, 1981)
(C) Visual acuity (cpd) Limit of visible frequency	46 (Van Hooser et al., 2005)	6 (Van Hooser et al., 2005)	3.7 (Hupfeld et al., 2006)	2.4 (Petry et al., 1984)	3 (Pak, 1984)	3.9 (Jacobs et al., 1982)	1.2 (Van Hooser et al., 2005)	0.56 (Van Hooser et al., 2005)
(C-1) Visual acuity (cpd) Frequency at optimized response/ performance	2.7 (Mazade and Alonso, 2017)	0.9 (Movshon et al., 1978)	0.22 (Baker et al., 1998; Dunn-Weiss et al., 2019)	0.26 (Johnson et al., 2010)	0.20 (Zhuang et al., 2013)	0.5 (Jacobs et al., 1982)	0.22 (Powers and Green, 1978)	0.04 (Niell and Stryker, 2008)
(D) Body weight (g)	8,000 (Van Hooser et al., 2005)	3,250 (Van Hooser et al., 2005)	800 (Van Hooser et al., 2005)	200 (Van Hooser et al., 2005)	2,720 (Howland et al., 2004)	600 (Van Hooser et al., 2005)	250 (Van Hooser et al., 2005)	25 (Van Hooser et al., 2005)
(E) Size ratio (A/B)	1.98	0.75	0.98	0.60	0.18	0.40	0.13	0.20
(F) 2D density of V1 neurons (cells/mm^2; see Figure S4 for details and references)	3,033	1,792	2,032	2,045	2,021 (average)	2,021 (average)	2,029	2,205
(G) Number of V1 neurons ($\times 10^3$; A × F)	3,812	681	169	149	162	166	14	7
(H) Number of RGC ($\times 10^3$)	1,600 (Ross and Kay, 2004)	247 (Ross and Kay, 2004)	90 (Henderson et al., 1988)	305 (Samuels et al., 2018)	550 (Robinson et al., 1987)	1,200 (Johnson et al., 1998)	110 (Ross and Kay, 2004)	70 (Ross and Kay, 2004)
(I) Cell number ratio, Φ (G/H)	2.38	2.76	1.87	0.49	0.29	0.14	0.13	0.09
(J) Sampling ratio, Γ ($0.76 \times S\sqrt{\Phi}$; see STAR Methods)	6.07	4.87	4.72	2.41	1.87	1.28	1.24	1.07

The size ratio (E) and cell number ratio (I) in the main text were estimated from previous experimental data in each case. To estimate the sampling ratio (J), the spatial period of preferred orientations (*S*) seeded in the retina is required. For cats, macaques, and mice, the spatial periods were estimated from the RGC mosaics data of each species (cat, 3.86 [Zhan and Troy, 2000]; mouse, 4.59 [Bleckert et al., 2014]; macaque, 5.17 [Vidne et al., 2012]; see STAR Methods and Figure S1C for details). For the other five species, the RGC mosaic data were not currently available. Therefore, the size of the retinal cluster was assumed to be the average of three representative values obtained from cats, monkeys, and mice ($S = 4.54$). Note that the visual acuity was measured by two different definitions in previous studies (C and C-1); neither of them can predict the V1 organization of diverse species. The 2D density of V1 neurons in rabbit and gray squirrel (F) was estimated from the average density of the other species (except macaques), based on the previous observation that the surface density of V1 neurons is not noticeably different across diverse species (except primates) (Srinivasan et al., 2015). See also Figure S4.

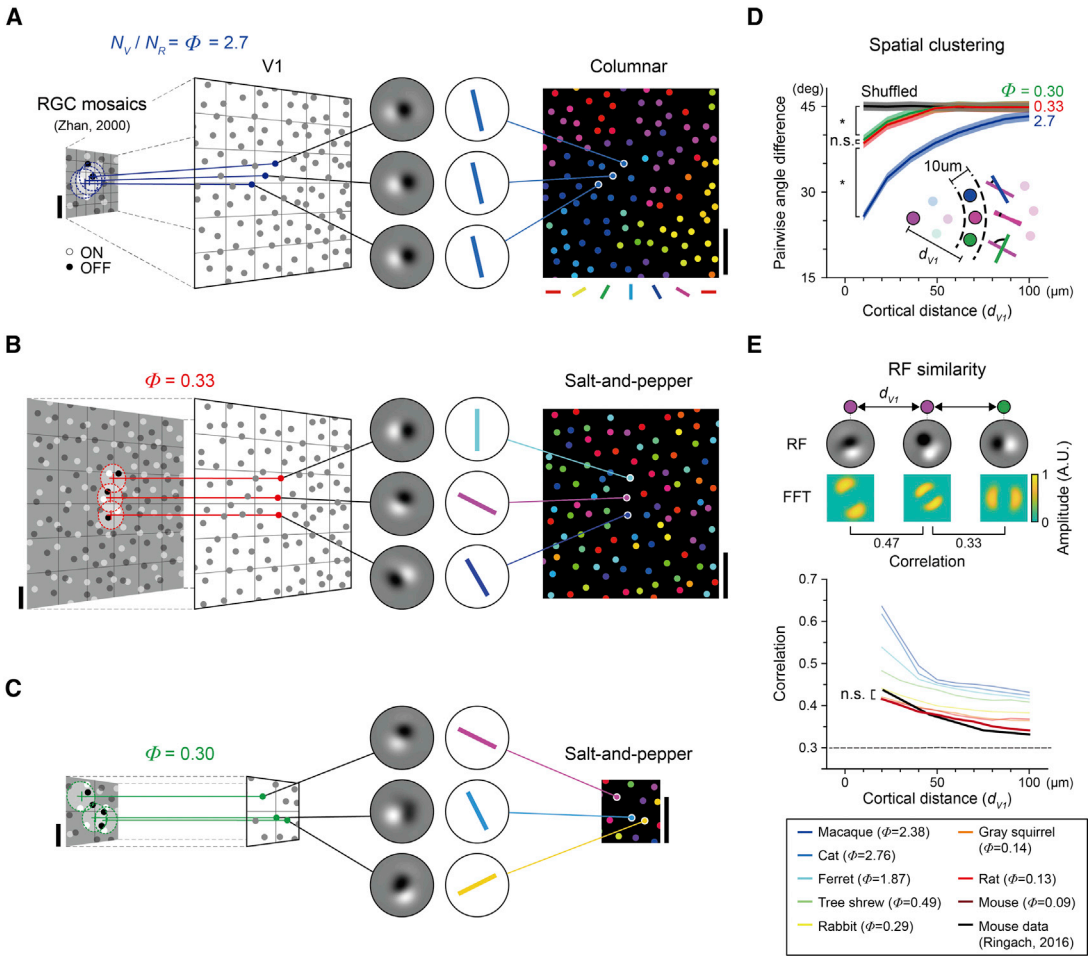

Figure 2. Variation of V1 Organizations with Retino-Cortical Mapping Conditions

(A–C) From given RGC mosaics, either columnar or salt-and-pepper organizations can be seeded according to the retino-cortical mapping condition.

(A) For a high mapping ratio between RGC and V1 neurons (Φ = 2.7), neighboring V1 neurons had highly overlapping receptive fields, resulting in a columnar organization of orientation tuning. Scale bar, 100 μm in retina and V1.

(B) When a larger retinal mosaic matches the same V1, the mapping ratio (Φ = 0.33) decreases and sparse sampling density induces weakly overlapping receptive fields of neighboring V1 neurons, resulting in a salt-and-pepper organization.

(C) A low mapping ratio (Φ = 0.30) can also be achieved due to small V1 size and generates a similar salt-and-pepper organization of orientation preference.

(D) Difference between the preferred orientation of neighboring V1 neurons: Φ = 2.7 versus Φ = 0.33 (blue versus red), *p = 6.0×10^{-4}; Φ = 0.30 versus Φ = 0.33 (green versus red), p = 0.43; Φ = 0.30 versus shuffled (green versus black), and *p = 2.1×10^{-2}; two-sample Kolmogorov-Smirnov test. Shaded areas indicate the SD of the orientation difference measured from all pairs of V1 neurons (Φ = 2.7, n = 5.66×10^{6}; Φ = 0.33, n = 8.27×10^{4}; Φ = 0.3, n = 6.82×10^{4} pairs from 100 repeated simulations).

(E) Top: example of tuning profiles of V1 receptive field obtained using the fast Fourier transform (FFT) analysis. Bottom: tuning similarity among neighboring neurons for different mapping conditions. Weakly clustered orientation tuning observed in mice (Ringach et al., 2016) is reproduced by the model (Φ = 0.09). Data versus Φ = 0.09 (black versus dark red), p = 0.23; two-sample Kolmogorov-Smirnov test.

See also Figures S1, S2, and S3.

(RF) of sampled RGCs (Ringach, 2007) (Figures S1A and S1B). We assumed that every cortical cell receives input from a similar number for RGCs regardless of variation in RGC density and retino-cortical magnification, because the density of the RGCs and retino-cortical magnification are proportional across retinal eccentricity in the observed RGC data at large scale (Chaplin et al., 2013; Peichl and Wässle, 1979; Stone, 1965; Wässle et al., 1990) (Figure S2).

When the mapping ratio between RGC and V1 neurons was high (Φ = 2.7; i.e., local RGCs are sampled by a large number of V1 neurons), neighboring V1 neurons had highly overlapping receptive fields due to a high sampling density of mapping from retina to V1 space (Figure 2A). Then, neighboring V1 neurons had similar orientation tuning, resulting in a columnar organization of orientation tuning (Figures 2A, right, and 2D, blue curve). In contrast, when we decreased the mapping ratio (Φ = 0.33) by matching a larger retinal mosaic to the same V1, neighboring V1 neurons received inputs from weakly overlapping RGC populations due to the sparse sampling density of the mapping (Figure 2B, left) and induced a salt-and-pepper organization

(Figures 2B, right and 2D, red curve; Φ = 2.7 versus 0.33 [blue versus red], *p = 6.0×10^{-4}; two-sample Kolmogorov-Smirnov test). We also observed similar salt-and-pepper organization when we decreased the mapping ratio (Φ = 0.30) by decreasing V1 size for the same RGC mosaics (Figures 2C, right and 2D, green curve; Φ = 0.30 versus 0.33 [green versus red], p = 0.43; two-sample Kolmogorov-Smirnov test). These results demonstrate that distinct V1 organizations can originate from different retino-cortical mapping ratios rather than from absolute size of RGC mosaics or V1. The results from comparison of these distinct mapping conditions explain why rabbits and gray squirrels do not have columnar clustering, while ferrets and tree shrews have columnar clustering, even though their V1 sizes are comparable (Figures 2A versus 2B).

Interestingly, we found that even for low Φ, V1 organization of orientation tuning can be slightly clustered as in mice (Kondo et al., 2016; Ringach et al., 2016) (Figure 2D, Φ = 0.30 versus shuffled [green versus black], *p = 2.1×10^{-2}; two-sample Kolmogorov-Smirnov test). This is because the sampling of neighboring V1 neurons can partially overlap in the retinal space (Jimenez et al., 2018). We found a condition of salt-and-pepper organization with weak clustering that quantitatively matched the statistics of pairwise tuning similarity (Figure 2E, top) in recent observations of salt-and-pepper organization in mice (Kondo et al., 2016; Ringach et al., 2016) (Figure 2E, bottom; data versus Φ = 0.09 as estimated for mice [black versus dark red], p = 0.23; two-sample Kolmogorov-Smirnov test). Thus, our model also provides a rationale for the observed local clustering in the salt-and-pepper organization of mice (Kondo et al., 2016; Ringach et al., 2016), gray squirrels (Van Hooser et al., 2005), and rabbits (Murphy and Berman, 1979). Note that our current model was tested using experimentally measured RGC mosaics instead of the regular hexagonal tiling of RGCs in the original Paik-Ringach model (Paik and Ringach, 2011, 2012). Hence, this demonstrates that the model works for a more general condition of retinal mosaics compared to that in our previous studies.

Species with or without Columnar Clustering Predicted from the Nyquist Theorem

Next, we examined the exact condition of the mapping ratio that generates columnar and salt-and-pepper organizations, respectively. For this, we applied a mathematical model for Nyquist sampling (Nyquist, 1928) to investigate how topographic information of underlying retinal mosaics pattern could be differently mapped onto cortical space, depending on the mapping ratio condition. According to the Nyquist theorem, sampling frequency should be higher than twice the frequency of the original signal to avoid aliasing. Thus, we assumed that the retino-cortical sampling ratio should be sufficiently high to generate columnar organization in V1 from the projection of the clustered retinal mosaics structure (Ringach, 2007). To validate this idea, we examined the retino-cortical mapping ratio that can initiate orientation pinwheels in the V1 organization, in which more than two cortical neurons are mapped between neighboring pinwheels distance in the columnar map. Using the estimated spatial period of orientation tuning seeded in the retinal mosaics, we predicted the distance between neighboring pinwheels (pinwheel distance) and examined whether more than two V1 neurons can be mapped within this distance for the mapping condition of each species. To do this quantitatively, we defined the retino-cortical sampling ratio (Γ = number of V1 neurons per pinwheel distance; see STAR Methods for details) instead of the mapping ratio (Φ) in the previous analysis, which only roughly compares the relative number of neurons.

We first estimated a topographic cluster pattern of orientation tuning in the cat RGC mosaics shown in Figure 2 (Zhan and Troy, 2000). From estimation of the local profile of ON and OFF RGC receptive fields (Figure 3A), orientation preference of the local neurons and the spatial periodicity of iso-orientation domains were simulated (period = 413 μm in RGC mosaics = 3.86 $d_{ON/OFF}$, where $d_{ON/OFF}$ indicates the expected average lattice distance of ON and OFF mosaics (0.107 mm); see Figures S1B and S1C for details). The nearest neighbor pinwheel distance was assumed to be 0.534 times the iso-domain period (413 μm × 0.534 = 221 μm in RGC mosaics) as reported in previous studies (Müller et al., 2000), because this cluster pattern does not contain enough pinwheels for the estimation of average distance. Similarly, the sizes of the retinal clusters in macaques (5.17 $d_{ON/OFF}$) and mice (4.59 $d_{ON/OFF}$) were estimated by analyzing RGC data obtained from each species (Bleckert et al., 2014; Vidne et al., 2012) (Figure S1). For the other five species, the RGC mosaic data were not currently available, thus the size of the retinal cluster was assumed to be the average of three representative values obtained from cats, monkeys, and mice (4.54 $d_{ON/OFF}$).

With this computational estimation of the retinal cluster, we investigated modulation of the cortical map structure, generated from mapping of the retinal cluster for various sampling ratio Γ. According to the Nyquist theorem (Nyquist, 1928), a low sampling ratio will cause an aliasing problem, thus our model predicts that parametric division of cortical organization will occur around the threshold Γ = 2. As expected, we observed that a high retina-to-cortex sampling ratio Γ (large V1) develops a periodic orientation map by projecting periodic RGC clusters onto the cortex with no sampling alias (Figure 3B, Γ = 6), while a low sampling ratio Γ (small V1) causes a noticeable aliasing of RGC periodicity, producing more irregular clustering of orientation tunings in neighboring V1 neurons (Figure 3B, Γ = 1.5).

From model simulations of various sampling ratios with RGC mosaics of three species (cat, macaque, and mouse), we confirmed that the local map continuity (or degree of spatial clustering) of orientation tuning increased with an increase in the retina-to-cortex sampling ratio Γ (Figures 3C and S1D–S1F), indicating a transition from the salt-and-pepper organization to a smooth columnar map. We observed that the model simulation of each species could reconstruct the V1 organization observed in the data (either salt-and-pepper or columnar organizations) from the same RGC mosaics. Importantly, when the average calculated angle difference was within 150 μm, approximately the range between the smallest orientation map period (520 μm, tree shrew) (Bosking et al., 1997) and the local clustering size in mice ($\approx$50 μm) (Kondo et al., 2016; Ringach et al., 2016), the transition between two organizations appeared to change abruptly around the sampling ratio of Γ = 2 (the Nyquist frequency; Figure 3C, top), explaining why cortical

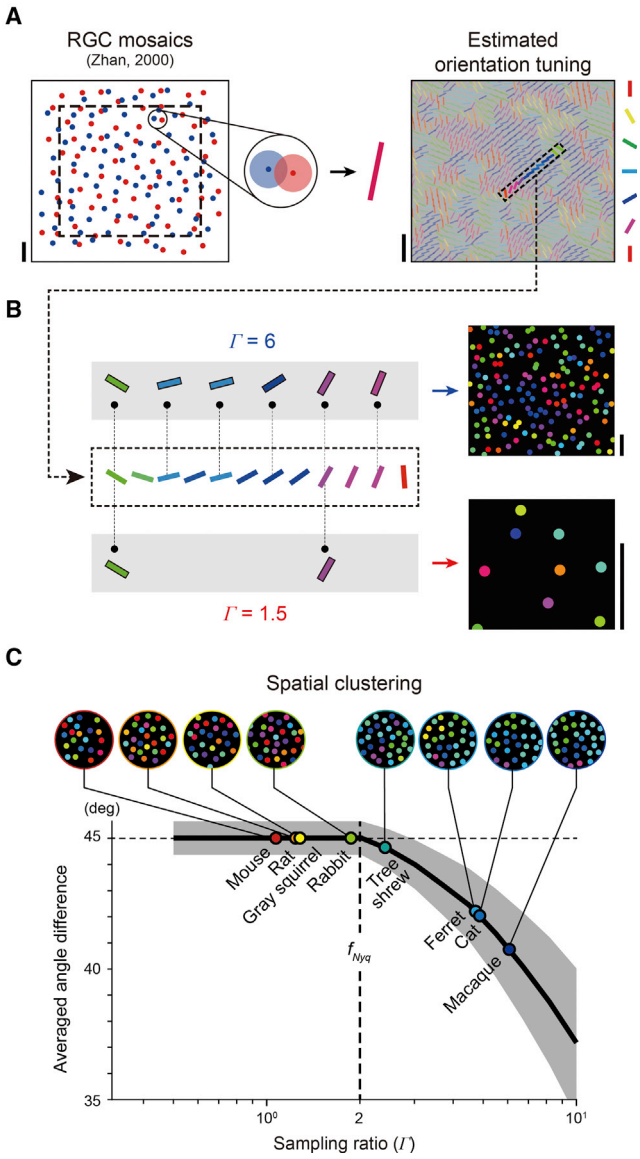

Figure 3. V1 Organization as a Nyquist Sampling in the Retino-Cortical Projection

(A) Expected cluster pattern of preferred orientation across retinal mosaics in Figure 2A. Scale bar, 100 μm in the retina.

(B) According to the Nyquist theorem, high ratio Γ (>2) of cortical sampling induces a continuous change of orientation tuning, while low Γ (<2) would cause an aliasing of RGC periodicity and an abrupt change of orientation tuning. Scale bar, 50 μm in V1.

(C) The model predicts that the organization of cortical orientation tuning makes a sharp transition around the Nyquist sampling frequency (f_{Nyq}), matching the observations of estimated sampling ratios across species. Shaded area indicates the standard deviation across diverse conditions of retino-cortical feedforward convergence (Figures S3E and S3F). Top: orientation tuning is distributed in random-like manner for Γ <2. As Γ increases (>2), the organization becomes more clustered, resulting in smaller angle difference among neighboring V1 neurons.

See also Figure S3.

organizations are observed in either columnar or salt-and-pepper organizations but not in intermediates between these two stages (Figures 3C and S1D–S1F). This abrupt transition becomes even sharper when a nonlinear neural response function is introduced, which suppresses the weak orientation tuning induced by noisy receptive fields (Figures S3A and S3B).

DISCUSSION

Our findings suggest that both columnar and salt-and-pepper organizations of cortical circuits originate from retinal mosaics and by a universal development process. A mathematical sampling model shows that retino-cortical mapping is a prime determinant of the topography of cortical organization and this prediction was confirmed by neural parameter analysis of data from eight species. This result implies that evolutionary variation of the size of retina and V1 has led to development of distinct topographical circuitry in V1, without species-specific developmental principles.

One can argue that the development of the salt-and-pepper organization in rodents originates from other characteristics of the rodent visual system, such as the diverse types of RGCs in mice (>32 types) (Baden et al., 2016). However, it was recently reported that the response of mouse LGN neurons is mainly modulated by two major types of RGCs (Román Rosón et al., 2019) and that this is similar in primates. In addition, the majority of these types of RGC is still classified as ON or OFF classes of RGC, and each single class of RGC has been observed to be tiled regularly across the retinal surface (Anishchenko et al., 2010; Baden et al., 2016) as in higher mammals, implying that the regularly structured RGC mosaics may develop cortical organizations in both higher mammals and rodents, resulting in blueprints for cortical topography.

Although larger receptive fields and lower visual acuity are noticeable features of the rodent visual system, cortical orientation tuning in rodents is also highly predictable according to the angle at which the ON and OFF inputs are aligned (Lien and Scanziani, 2013), similar to higher mammals (Jin et al., 2011; Kremkow et al., 2016; Lee et al., 2016). This implies that the arrangement of neighboring ON and OFF feedforward afferents is a more critical factor determining the organization of orientation tuning than the size of each input component, as supported by our additional simulation with enlarged RGC receptive fields (Figures S3C and S3D). The results of a comparison of the visual acuity of gray squirrels (3.4 cycle per degree [cpd]; without orientation columns) and that of tree shrews (2.4 cpd; with orientation columns) also suggest that large receptive fields or low visual acuity are not predictors of the salt-and-pepper organization.

The large convergence in the retino-thalamic pathway in rodents is another factor to be considered. Electron microscopy techniques revealed that axons from several dozen RGCs anatomically innervated an LGN neuron in a mouse (Morgan et al., 2016), while LGN neurons in cats (Usrey et al., 1999; Yeh et al., 2009) or macaques (Schein and de Monasterio, 1987) appear to receive inputs from less than 8 RGCs on average. Therefore, this greater convergence in rodents has been considered to interrupt the development of a columnar organization in V1 (Jang and Paik, 2017; Sailamul et al., 2017). However, in a recent study of mice in which the functional connectome

between the retina and the LGN was examined, it was reported that the LGN neuron activity is mainly modulated by three RGC inputs on average (Litvina and Chen, 2017) and that this is in similar in cats and macaques. In addition, the receptive fields of mouse V1 neurons mostly consist of a couple of ON and OFF subregions (Bonin et al., 2011; Smith and Häusser, 2010), implying that the functional connectome of retino-cortical pathways might be more similarly structured across species than is predictable from an anatomical connectome. Our simulation results also support this idea, showing that orientation tuning of a V1 neuron remains consistent even with variation of the convergence range, because the tuning is predominantly determined by a couple of ON and OFF RGCs near the center of the convergence mapping in retinal space (Figures S3E and S3F).

Previous studies also suggest that the emergence of orientation tuning in the earlier developmental stage of the visual pathway in rodents can provide evidence of the source of the salt-and-pepper organization (Scholl et al., 2013). However, most orientation-tuned cells in the retina (Nath and Schwartz, 2017) and LGN (Tang et al., 2016) are either ON or OFF types, while most orientation-tuned V1 neurons contain both ON and OFF subregions in their receptive fields (Cossell et al., 2015; Niell and Stryker, 2008). Thus, the major thalamic inputs to V1 still consist of untuned units (Niell, 2013), and LGN orientation-selective cells are not the primary source of orientation tuning in V1. Importantly, the preferred orientation of V1 neurons in mice is highly predictable from the alignment between the ON and OFF receptive fields (Lien and Scanziani, 2013), implying that cortical orientation tuning in rodents is initiated by the integration of ON and OFF feedforward inputs rather than by orientation tuning in the retina or LGN. Our additional simulation also supports this idea, showing that the cortical organization of orientation tuning remains consistent even with elliptical RGC receptive fields having weak orientation tuning (Zhao et al., 2013) (Figures S3G–S3I).

One can argue that each V1 organization may originate from the different dynamics of recurrent cortical circuits across species, but experimental observations provide evidence that the cortical organization of orientation tuning is initialized by feedforward afferents rather than by recurrent circuits (Jin et al., 2011). It was recently reported that orientation tuning is initially seeded by randomly sampled ON and OFF feedforward afferents, and recurrent circuits can modulate further refinement of the receptive field (Pattadkal et al., 2018). Indeed, cortical orientation tuning and its columnar organization are observed before the complete development of recurrent circuits, and the spatial layout of this initial organization is maintained through the development stage (Chapman et al., 1996; Crair et al., 1998; Huberman et al., 2008). This indicates that the cortical organization of orientation tuning is initially seeded by feedforward afferents and can be fine-tuned by various types of synaptic plasticity in feedforward and recurrent circuits (Park et al., 2017; Lee et al., 2020).

Note that the current study is based on a comparative study of only eight species, and additional investigations of other species will provide further support for our model. For example, the galago (bush baby) is another primate species with orientation columns (Xu et al., 2005). Although its anatomic parameters are seemingly different from that of macaques (retina size, 332 [Kaas and Collins, 2005] versus 636 mm^2; V1 size, 212 [Rosa et al., 1997] versus 1,257 mm^2), our model predicts that this species would have orientation columns because the ratio between the size of V1 and the retina (212/332 = 0.64) has been found to be a condition initiating the columnar organization (>0.46; Figure 1C), consistent with experimental observations. In addition, ongoing observations of orientation columns in wallabies (Jung et al., 2019) may provide additional datasets with which to test our model predictions.

A key assumption of the current model is that neighboring V1 neurons receive feedforward inputs from a similar population of nearby RGCs, as suggested by the statistical wiring model (Ringach, 2004, 2007). Although such feedforward projections have not yet been directly measured due to a lack of experimental techniques capable of tracing the retino-cortical connectome while also measuring corresponding receptive fields, recent studies have reported a vestige of such local pooling, where the location ON and OFF receptive fields of neighboring V1 neurons are highly clustered, resulting in similar orientation preference of these neurons (Kremkow et al., 2016; Lee et al., 2016). Considering that the ON and OFF topology in V1 originates from the thalamic afferents (Jin et al., 2011) and that most thalamic neurons relay retinal afferents (Usrey et al., 1999), these results suggest that neighboring V1 neurons receive ON and OFF retinal inputs from a similar population of nearby RGCs.

Although the manner by which each V1 organization is projected onto the next stage has not yet been directly measured, previous studies suggest distinct functional impacts of the two organizations on further visual pathways. In a salt-and-pepper organization, orientation tuning is distributed in a random-like manner such that receptive fields with different preferred orientations can sample a visual scene more uniformly (Kaschube, 2014). Considering that connections from rodent V1 project to very different visual areas (Andermann et al., 2011; Garrett et al., 2014; Wang and Burkhalter, 2007), the salt-and-pepper organization may be the structure providing unbiased visual inputs for diverse visual pathways specialized for distinct visual functions, such as motion-related versus pattern-related computations (Marshel et al., 2011). In contrast, local orientation tuning in a columnar organization is more biased toward a specific orientation, but this structure enables an efficient tiling of diverse functional modules for ocular dominance or spatial frequency tuning, maximizing the representation of different stimulus combinations for each cortical location (Nauhaus et al., 2016; Swindale et al., 2000).

The functional role of the columnar and salt-and-pepper organization has been debated (Koch et al., 2016; Li et al., 2019), and future studies are needed to reveal whether each type of organization is the optimized form of functional circuits under different physical constraints in each species. Our findings may provide advanced insight into the study of distinct cortical architectures under a universal principle of development process.

STAR★METHODS

Detailed methods are provided in the online version of this paper and include the following:

- KEY RESOURCES TABLE
- LEAD CONTACT AND MATERIALS AVAILABILITY

- EXPERIMENTAL MODEL AND SUBJECT DETAILS
- METHOD DETAILS
  - Analysis of anatomical data
  - Estimation of retino-cortical sampling ratio
  - Connectivity and receptive field models
  - Measurement of cortical functional tuning
- QUANTIFICATION AND STATISTICAL ANALYSIS
- DATA AND CODE AVAILABILITY

SUPPLEMENTAL INFORMATION

Supplemental Information can be found online at https://doi.org/10.1016/j.celrep.2020.02.038.

ACKNOWLEDGMENTS

We are grateful to Jose-Manuel Alonso, Matteo Carandini, Dario Ringach, John Murray, and Daeyeol Lee for discussing and providing comments on earlier versions of this manuscript. This work was supported by National Research Foundation of Korea (NRF) grants (NRF-2016R1C1B2016039, NRF-2019R1A2C4069863, and NRF-2019M3E5D2A01058328 to S.-B.P.) funded by the Korea government (MSIT).

AUTHOR CONTRIBUTIONS

S.-B.P. conceived the project. J.J., M.S., and S.-B.P. designed the model. J.J. and M.S. performed the simulations. J.J., M.S., and S.-B.P. analyzed the data. J.J., M.S., and S.-B.P. wrote the manuscript.

DECLARATION OF INTERESTS

The authors declare no competing interests.

Received: September 20, 2019
Revised: December 27, 2019
Accepted: February 7, 2020
Published: March 10, 2020

REFERENCES

Adams, D.L., Sincich, L.C., and Horton, J.C. (2007). Complete pattern of ocular dominance columns in human primary visual cortex. J. Neurosci. *27*, 10391–10403.

Andermann, M.L., Kerlin, A.M., Roumis, D.K., Glickfeld, L.L., and Reid, R.C. (2011). Functional specialization of mouse higher visual cortical areas. Neuron *72*, 1025–1039.

Anishchenko, A., Greschner, M., Elstrott, J., Sher, A., Litke, A.M., Feller, M.B., and Chichilnisky, E.J. (2010). Receptive field mosaics of retinal ganglion cells are established without visual experience. J. Neurophysiol. *103*, 1856–1864.

Ayzenshtat, I., Jackson, J., and Yuste, R. (2016). Orientation tuning depends on spatial frequency in mouse visual cortex. eNeuro *3*, 1–12.

Baden, T., Berens, P., Franke, K., Román Rosón, M., Bethge, M., and Euler, T. (2016). The functional diversity of retinal ganglion cells in the mouse. Nature *529*, 345–350.

Baker, G.E., Thompson, I.D., Krug, K., Smyth, D., and Tolhurst, D.J. (1998). Spatial-frequency tuning and geniculocortical projections in the visual cortex (areas 17 and 18) of the pigmented ferret. Eur. J. Neurosci. *10*, 2657–2668.

Balasubramanian, V., and Sterling, P. (2009). Receptive fields and functional architecture in the retina. J. Physiol. *587*, 2753–2767.

Blasdel, G.G., and Salama, G. (1986). Voltage-sensitive dyes reveal a modular organization in monkey striate cortex. Nature *321*, 579–585.

Bleckert, A., Schwartz, G.W., Turner, M.H., Rieke, F., and Wong, R.O.L. (2014). Visual space is represented by nonmatching topographies of distinct mouse retinal ganglion cell types. Curr. Biol. *24*, 310–315.

Bock, D.D., Lee, W.-C.A., Kerlin, A.M., Andermann, M.L., Hood, G., Wetzel, A.W., Yurgenson, S., Soucy, E.R., Kim, H.S., and Reid, R.C. (2011). Network anatomy and in vivo physiology of visual cortical neurons. Nature *471*, 177–182.

Bonin, V., Histed, M.H., Yurgenson, S., and Reid, R.C. (2011). Local diversity and fine-scale organization of receptive fields in mouse visual cortex. J. Neurosci. *31*, 18506–18521.

Bosking, W.H., Zhang, Y., Schofield, B., and Fitzpatrick, D. (1997). Orientation selectivity and the arrangement of horizontal connections in tree shrew striate cortex. J. Neurosci. *17*, 2112–2127.

Ch'ng, Y.H., and Reid, R.C. (2010). Cellular imaging of visual cortex reveals the spatial and functional organization of spontaneous activity. Front. Integr. Neurosci. *4*, 1–9.

Chaplin, T.A., Yu, H.-H., and Rosa, M.G.P. (2013). Representation of the visual field in the primary visual area of the marmoset monkey: magnification factors, point-image size, and proportionality to retinal ganglion cell density. J. Comp. Neurol. *521*, 1001–1019.

Chapman, B., Stryker, M.P., and Bonhoeffer, T. (1996). Development of orientation preference maps in ferret primary visual cortex. J. Neurosci. *16*, 6443–6453.

Cossell, L., Iacaruso, M.F., Muir, D.R., Houlton, R., Sader, E.N., Ko, H., Hofer, S.B., and Mrsic-Flogel, T.D. (2015). Functional organization of excitatory synaptic strength in primary visual cortex. Nature *518*, 399–403.

Crair, M.C., Gillespie, D.C., and Stryker, M.P. (1998). The role of visual experience in the development of columns in cat visual cortex. Science *279*, 566–570.

Croner, L.J., and Kaplan, E. (1995). Receptive fields of P and M ganglion cells across the primate retina. Vision Res. *35*, 7–24.

Ding, Y., Zheng, Y., Liu, T., Chen, T., Wang, C., Sun, Q., Hua, M., and Hua, T. (2017). Changes in GABAergic markers accompany degradation of neuronal function in the primary visual cortex of senescent rats. Sci. Rep. *7*, 14897.

Dräger, U.C., and Olsen, J.F. (1981). Ganglion cell distribution in the retina of the mouse. Invest. Ophthalmol. Vis. Sci. *20*, 285–293.

Dunn-Weiss, E., Nummela, S.U., Lempel, A.A., Law, J.M., Ledley, J., Salvino, P., and Nielsen, K.J. (2019). Visual Motion and Form Integration in the Behaving Ferret. Eneuro *6*, ENEURO.0228-19.2019.

Engelmann, R., and Peichl, L. (1996). Unique distribution of somatostatin-immunoreactive cells in the retina of the tree shrew (Tupaia belangeri). Eur. J. Neurosci. *8*, 220–228.

Espinoza, S.G., and Thomas, H.C. (1983). Retinotopic organization of striate and extrastriate visual cortex in the hooded rat. Brain Res. *272*, 137–144.

Garrett, M.E., Nauhaus, I., Marshel, J.H., and Callaway, E.M. (2014). Topography and areal organization of mouse visual cortex. J. Neurosci. *34*, 12587–12600.

Goltstein, P.M., Coffey, E.B.J., Roelfsema, P.R., and Pennartz, C.M.A. (2013). In vivo two-photon Ca2+ imaging reveals selective reward effects on stimulus-specific assemblies in mouse visual cortex. J. Neurosci. *33*, 11540–11555.

Henderson, Z. (1985). Distribution of ganglion cells in the retina of adult pigmented ferret. Brain Res. *358*, 221–228.

Henderson, Z., Finlay, B.L., and Wikler, K.C. (1988). Development of ganglion cell topography in ferret retina. J. Neurosci. *8*, 1194–1205.

Howland, H.C., Merola, S., and Basarab, J.R. (2004). The allometry and scaling of the size of vertebrate eyes. Vision Res. *44*, 2043–2065.

Huberman, A.D., Feller, M.B., and Chapman, B. (2008). Mechanisms underlying development of visual maps and receptive fields. Annu. Rev. Neurosci. *31*, 479–509.

Hughes, A. (1971). Topographical relationships between the anatomy and physiology of the rabbit visual system. Doc. Ophthalmol. *30*, 33–159.

Hughes, A. (1975). A quantitative analysis of the cat retinal ganglion cell topography. J. Comp. Neurol. *163*, 107–128.

Hughes, A. (1979). A schematic eye for the rat. Vision Res. *19*, 569–588.

Hupfeld, D., Distler, C., and Hoffmann, K.-P. (2006). Motion perception deficits in albino ferrets (Mustela putorius furo). Vision Res. *46*, 2941–2948.

Jacobs, G.H., Birch, D.G., and Blakeslee, B. (1982). Visual acuity and spatial contrast sensitivity in tree squirrels. Behav. Processes *7*, 367–375.

Jang, J., and Paik, S.B. (2017). Interlayer repulsion of retinal ganglion cell mosaics regulates spatial organization of functional maps in the visual cortex. J. Neurosci. *37*, 12141–12152.

Jimenez, L.O., Tring, E., Trachtenberg, J.T., and Ringach, D.L. (2018). Local tuning biases in mouse primary visual cortex. J. Neurophysiol. *120*, 274–280.

Jin, J., Wang, Y., Swadlow, H.A., and Alonso, J.M. (2011). Population receptive fields of ON and OFF thalamic inputs to an orientation column in visual cortex. Nat. Neurosci. *14*, 232–238.

Johnson, P.T., Geller, S.F., and Reese, B.E. (1998). Distribution, size and number of axons in the optic pathway of ground squirrels. Exp. Brain Res. *118*, 93–104.

Johnson, E.N., Van Hooser, S.D., and Fitzpatrick, D. (2010). The representation of S-cone signals in primary visual cortex. J. Neurosci. *30*, 10337–10350.

Jung, Y., Yunzab, M., Almasi, A., Sun, S., Cloherty, S., Bauquier, S., Renfree, M., Meffin, H., and Ibbotson, M. (2019). Orientation maps in the primary visual cortex of an Australian marsupial, the Tammar Wallaby Macropus eugenii. Program No. 754.21. 2019 Neuroscience Meeting Planner (Society for Neuroscience).

Kaas, J.H., and Collins, C.E. (2005). The Primate Visual System (Wiley).

Kaschube, M. (2014). Neural maps versus salt-and-pepper organization in visual cortex. Curr. Opin. Neurobiol. *24*, 95–102.

Kaschube, M., Schnabel, M., Löwel, S., Coppola, D.M., White, L.E., and Wolf, F. (2010). Universality in the evolution of orientation columns in the visual cortex. Science *330*, 1113–1116.

Keil, W., Kaschube, M., Schnabel, M., Kisvarday, Z.F., Lowel, S., Coppola, D.M., White, L.E., and Wolf, F. (2012). Response to comment on "Universality in the evolution of orientation columns in the visual cortex.". Science *336*, 413.

Kimura, R., Safari, M.-S., Mirnajafi-Zadeh, J., Kimura, R., Ebina, T., Yanagawa, Y., Sohya, K., and Tsumoto, T. (2014). Curtailing effect of awakening on visual responses of cortical neurons by cholinergic activation of inhibitory circuits. J. Neurosci. *34*, 10122–10133.

Koch, E., Jin, J., Alonso, J.M., and Zaidi, Q. (2016). Functional implications of orientation maps in primary visual cortex. Nat. Commun. *7*, 13529.

Kondo, S., Yoshida, T., and Ohki, K. (2016). Mixed functional microarchitectures for orientation selectivity in the mouse primary visual cortex. Nat. Commun. *7*, 13210.

Kong, X., Wang, K., Sun, X., and Witt, R.E. (2010). Comparative study of the retinal vessel anatomy of rhesus monkeys and humans. Clin. Exp. Ophthalmol. *38*, 629–634.

Kremkow, J., Jin, J., Wang, Y., and Alonso, J.M. (2016). Principles underlying sensory map topography in primary visual cortex. Nature *533*, 52–57.

Law, M.I., Zahs, K.R., and Stryker, M.P. (1988). Organization of primary visual cortex (area 17) in the ferret. J. Comp. Neurol. *278*, 157–180.

Lee, K.-S., Huang, X., and Fitzpatrick, D. (2016). Topology of ON and OFF inputs in visual cortex enables an invariant columnar architecture. Nature *533*, 90–94.

Lee, H., Choi, W., Park, Y., and Paik, S.B. (2020). Distinct role of flexible and stable encodings in sequential working memory. Neural Netw. *121*, 419–429.

Li, Y., Van Hooser, S.D., Mazurek, M., White, L.E., and Fitzpatrick, D. (2008). Experience with moving visual stimuli drives the early development of cortical direction selectivity. Nature *456*, 952–956.

Li, M., Song, X.M., Xu, T., Hu, D., Roe, A.W., and Li, C. (2019). Subdomains within orientation columns of primary visual cortex. Sci. Adv. *5*, eaaw0807.

Lien, A.D., and Scanziani, M. (2013). Tuned thalamic excitation is amplified by visual cortical circuits. Nat. Neurosci. *16*, 1315–1323.

Litvina, E.Y., and Chen, C. (2017). Functional Convergence at the Retinogeniculate Synapse. Neuron *96*, 330–338.

Marshel, J.H., Garrett, M.E., Nauhaus, I., and Callaway, E.M. (2011). Functional specialization of seven mouse visual cortical areas. Neuron *72*, 1040–1054.

Mazade, R., and Alonso, J.M. (2017). Thalamocortical processing in vision. Vis. Neurosci. *34*, E007.

Meng, Y., Tanaka, S., and Poon, C.-S. (2012). Comment on "Universality in the evolution of orientation columns in the visual cortex". Science *336*, 413.

Moeyaert, B., Holt, G., Madangopal, R., Perez-Alvarez, A., Fearey, B.C., Trojanowski, N.F., Ledderose, J., Zolnik, T.A., Das, A., Patel, D., et al. (2018). Improved methods for marking active neuron populations. Nat. Commun. *9*, 4440.

Morgan, J.L., Berger, D.R., Wetzel, A.W., and Lichtman, J.W. (2016). The fuzzy logic of network connectivity in mouse visual thalamus. Cell *165*, 192–206.

Movshon, J.A., Thompson, I.D., and Tolhurst, D.J. (1978). Spatial and temporal contrast sensitivity of neurones in areas 17 and 18 of the cat's visual cortex. J. Physiol. *283*, 101–120.

Muir, D.R., and Kampa, B.M. (2015). FocusStack and StimServer: a new open source MATLAB toolchain for visual stimulation and analysis of two-photon calcium neuronal imaging data. Front. Neuroinform. *8*, 85.

Müller, T., Stetter, M., Hübener, M., Sengpiel, F., Bonhoeffer, T., Gödecke, I., Chapman, B., Löwel, S., and Obermayer, K. (2000). An analysis of orientation and ocular dominance patterns in the visual cortex of cats and ferrets. Neural Comput. *12*, 2573–2595.

Murphy, E.H., and Berman, N. (1979). The rabbit and the cat: a comparison of some features of response properties of single cells in the primary visual cortex. J. Comp. Neurol. *188*, 401–427.

Nath, A., and Schwartz, G.W. (2017). Electrical synapses convey orientation selectivity in the mouse retina. Nat. Commun. *8*, 2025.

Nauhaus, I., Nielsen, K.J., Disney, A.A., and Callaway, E.M. (2012). Orthogonal micro-organization of orientation and spatial frequency in primate primary visual cortex. Nat. Neurosci. *15*, 1683–1690.

Nauhaus, I., Nielsen, K.J., and Callaway, E.M. (2016). Efficient receptive field tiling in primate V1. Neuron *91*, 893–904.

Niell, C.M. (2013). Vision: more than expected in the early visual system. Curr. Biol. *23*, R681–R684.

Niell, C.M., and Stryker, M.P. (2008). Highly selective receptive fields in mouse visual cortex. J. Neurosci. *28*, 7520–7536.

Nyquist, H. (1928). Certain topics in telegraph transmission theory. Trans. Am. Inst. Electr. Eng. *47*, 617–644.

Ohki, K., Chung, S., Ch'ng, Y.H., Kara, P., and Reid, R.C. (2005). Functional imaging with cellular resolution reveals precise micro-architecture in visual cortex. Nature *433*, 597–603.

Ohki, K., Chung, S., Kara, P., Hübener, M., Bonhoeffer, T., and Reid, R.C. (2006). Highly ordered arrangement of single neurons in orientation pinwheels. Nature *442*, 925–928.

Oyster, C.W., Takahashi, E.S., and Hurst, D.C. (1981). Density, soma size, and regional distribution of rabbit retinal ganglion cells. J. Neurosci. *1*, 1331–1346.

Paik, S.B., and Ringach, D.L. (2011). Retinal origin of orientation maps in visual cortex. Nat. Neurosci. *14*, 919–925.

Paik, S.B., and Ringach, D.L. (2012). Link between orientation and retinotopic maps in primary visual cortex. Proc. Natl. Acad. Sci. USA *109*, 7091–7096.

Pak, M.A. (1984). Ocular refraction and visual contrast sensitivity of the rabbit, determined by the VECP. Vision Res. *24*, 341–345.

Palagina, G., Meyer, J.F., and Smirnakis, S.M. (2017). Complex visual motion representation in mouse area V1. J. Neurosci. *37*, 164–183.

Paninski, L., Pillow, J., and Lewi, J. (2007). Statistical models for neural encoding, decoding, and optimal stimulus design. Prog. Brain Res. *165*, 493–507.

Park, Y., Choi, W., and Paik, S.B. (2017). Symmetry of learning rate in synaptic plasticity modulates formation of flexible and stable memories. Sci. Rep. *7*, 5671.

Pattadkal, J.J., Mato, G., van Vreeswijk, C., Priebe, N.J., and Hansel, D. (2018). Emergent Orientation Selectivity from Random Networks in Mouse Visual Cortex. Cell Rep. *24*, 2042–2050.

Peichl, L., and Wässle, H. (1979). Size, scatter and coverage of ganglion cell receptive field centres in the cat retina. J. Physiol. *291*, 117–141.

Petry, H.M., Fox, R., and Casagrande, V.A. (1984). Spatial contrast sensitivity of the tree shrew. Vision Res. *24*, 1037–1042.

Philips, R.T., Sur, M., and Chakravarthy, V.S. (2017). The influence of astrocytes on the width of orientation hypercolumns in visual cortex: A computational perspective. PLoS Comput. Biol. *13*, e1005785.

Powers, M.K., and Green, D.G. (1978). Single retinal ganglion cell responses in the dark-reared rat: grating acuity, contrast sensitivity, and defocusing. Vision Res. *18*, 1533–1539.

Ringach, D.L. (2004). Haphazard wiring of simple receptive fields and orientation columns in visual cortex. J. Neurophysiol. *92*, 468–476.

Ringach, D.L. (2007). On the origin of the functional architecture of the cortex. PLoS ONE *2*, e251.

Ringach, D.L., Mineault, P.J., Tring, E., Olivas, N.D., Garcia-Junco-Clemente, P., and Trachtenberg, J.T. (2016). Spatial clustering of tuning in mouse primary visual cortex. Nat. Commun. *7*, 12270.

Robinson, S.R., Horsburgh, G.M., Dreher, B., and McCall, M.J. (1987). Changes in the numbers of retinal ganglion cells and optic nerve axons in the developing albino rabbit. Brain Res. *432*, 161–174.

Román Rosón, M., Bauer, Y., Kotkat, A.H., Berens, P., Euler, T., and Busse, L. (2019). Mouse dLGN Receives Functional Input from a Diverse Population of Retinal Ganglion Cells with Limited Convergence. Neuron *102*, 462–476.e8.

Rosa, M.G.P., Casagrande, V.A., Preuss, T., and Kaas, J.H. (1997). Visual field representation in striate and prestriate cortices of a prosimian primate (Galago garnetti). J. Neurophysiol. *77*, 3193–3217.

Ross, C.F., and Kay, R.F. (2004). Anthropoid Origins: New Visions (Springer US).

Sailamul, P., Jang, J., and Paik, S.B. (2017). Synaptic convergence regulates synchronization-dependent spike transfer in feedforward neural networks. J. Comput. Neurosci. *43*, 189–202.

Samuels, B.C., Siegwart, J.T., Zhan, W., Hethcox, L., Chimento, M., Whitley, R., Downs, J.C., and Girkin, C.A. (2018). A novel tree shrew (Tupaia belangeri) model of glaucoma. Invest. Ophthalmol. Vis. Sci. *59*, 3136–3143.

Schein, S.J., and de Monasterio, F.M. (1987). Mapping of retinal and geniculate neurons onto striate cortex of macaque. J. Neurosci. *7*, 996–1009.

Scholl, B., Tan, A.Y.Y., Corey, J., and Priebe, N.J. (2013). Emergence of orientation selectivity in the Mammalian visual pathway. J. Neurosci. *33*, 10616–10624.

Sesma, M.A., Casagrande, V.A., and Kaas, J.H. (1984). Cortical connections of area 17 in tree shrews. J. Comp. Neurol. *230*, 337–351.

Smith, S.L., and Häusser, M. (2010). Parallel processing of visual space by neighboring neurons in mouse visual cortex. Nat. Neurosci. *13*, 1144–1149.

Srinivasan, S., Carlo, C.N., and Stevens, C.F. (2015). Predicting visual acuity from the structure of visual cortex. Proc. Natl. Acad. Sci. USA *112*, 7815–7820.

Stone, J. (1965). A quantitative analysis of the distribution of ganglion cells in the cat's retina. J. Comp. Neurol. *124*, 337–352.

Sun, W., Tan, Z., Mensh, B.D., and Ji, N. (2016). Thalamus provides layer 4 of primary visual cortex with orientation- and direction-tuned inputs. Nat. Neurosci. *19*, 308–315.

Swindale, N.V., Shoham, D., Grinvald, A., Bonhoeffer, T., and Hübener, M. (2000). Visual cortex maps are optimized for uniform coverage. Nat. Neurosci. *3*, 822–826.

Tang, J., Ardila Jimenez, S.C., Chakraborty, S., and Schultz, S.R. (2016). Visual Receptive Field Properties of Neurons in the Mouse Lateral Geniculate Nucleus. PLoS ONE *11*, e0146017.

Tusa, R.J., Palmer, L.A., and Rosenquist, A.C. (1978). The retinotopic organization of area 17 (striate cortex) in the cat. J. Comp. Neurol. *177*, 213–235.

Usrey, W.M., Reppas, J.B., and Reid, R.C. (1999). Specificity and strength of retinogeniculate connections. J. Neurophysiol. *82*, 3527–3540.

Van Hooser, S.D., Heimel, J.A.F., Chung, S., Nelson, S.B., and Toth, L.J. (2005). Orientation selectivity without orientation maps in visual cortex of a highly visual mammal. J. Neurosci. *25*, 19–28.

Vidne, M., Ahmadian, Y., Shlens, J., Pillow, J.W., Kulkarni, J., Litke, A.M., Chichilnisky, E.J., Simoncelli, E., and Paninski, L. (2012). Modeling the impact of common noise inputs on the network activity of retinal ganglion cells. J. Comput. Neurosci. *33*, 97–121.

Wang, Q., and Burkhalter, A. (2007). Area map of mouse visual cortex. J. Comp. Neurol. *502*, 339–357.

Wang, K.H., Majewska, A., Schummers, J., Farley, B., Hu, C., Sur, M., and Tonegawa, S. (2006). In vivo two-photon imaging reveals a role of arc in enhancing orientation specificity in visual cortex. Cell *126*, 389–402.

Wässle, H., Grünert, U., Röhrenbeck, J., and Boycott, B.B. (1990). Retinal ganglion cell density and cortical magnification factor in the primate. Vision Res. *30*, 1897–1911.

Weigand, M., Sartori, F., and Cuntz, H. (2017). Universal transition from unstructured to structured neural maps. Proc. Natl. Acad. Sci. USA *114*, E4057–E4064.

Xu, X., Bosking, W.H., White, L.E., Fitzpatrick, D., and Casagrande, V.A. (2005). Functional organization of visual cortex in the prosimian bush baby revealed by optical imaging of intrinsic signals. J. Neurophysiol. *94*, 2748–2762.

Yeh, C.-I., Stoelzel, C.R., Weng, C., and Alonso, J.-M. (2009). Functional consequences of neuronal divergence within the retinogeniculate pathway. J. Neurophysiol. *101*, 2166–2185.

Yoshida, T., Ozawa, K., and Tanaka, S. (2012). Sensitivity profile for orientation selectivity in the visual cortex of goggle-reared mice. PLoS ONE *7*, e40630.

Zhan, X.J., and Troy, J.B. (2000). Modeling cat retinal beta-cell arrays. Vis. Neurosci. *17*, 23–39.

Zhao, X., Chen, H., Liu, X., and Cang, J. (2013). Orientation-selective responses in the mouse lateral geniculate nucleus. J. Neurosci. *33*, 12751–12763.

Zhuang, J., Stoelzel, C.R., Bereshpolova, Y., Huff, J.M., Hei, X., Alonso, J.-M., and Swadlow, H.A. (2013). Layer 4 in primary visual cortex of the awake rabbit: contrasting properties of simple cells and putative feedforward inhibitory interneurons. J. Neurosci. *33*, 11372–11389.

STAR★METHODS

KEY RESOURCES TABLE

REAGENT or RESOURCE	SOURCE	IDENTIFIER
Software and Algorithms		
MATLAB 2017a	The MathWorks, Inc.	RRID:SCR_001622

LEAD CONTACT AND MATERIALS AVAILABILITY

Further information and requests for resources should be directed to and will be fulfilled by the Lead Contact, Se-Bum Paik (sbpaik@kaist.ac.kr). This study did not generate new unique reagents.

EXPERIMENTAL MODEL AND SUBJECT DETAILS

The anatomical data used in this study were from Adams et al. (2007), Van Hooser et al. (2005), Kong et al. (2010), Nauhaus et al. (2016), Ross and Kay (2004), Nauhaus et al. (2012) for macaque; from Van Hooser et al. (2005), Hughes (1975), Ohki et al. (2005), Ross and Kay (2004), Tusa et al. (1978), Ohki et al., (2006) for cat; from Henderson (1985), Henderson et al. (1988), Van Hooser et al. (2005), Hupfeld et al. (2006), Law et al. (1988), Li et al. (2008), Sun et al. (2016) for ferret; from Engelmann and Peichl (1996), Van Hooser et al. (2005), Johnson et al. (2010), Keil et al. (2012), Samuels et al. (2018), Sesma et al. (1984) for tree shrew; from Howland et al. (2004), Hughes (1971), Oyster et al. (1981), Pak (1984), Ross and Kay (2004) for rabbit; from Van Hooser et al. (2005), Johnson et al. (1998), Ross and Kay (2004) for gray squirrel; from Espinoza and Thomas (1983), Van Hooser et al. (2005), Hughes (1979), Ohki et al. (2005), Ross and Kay (2004), Ch'ng and Reid (2010), Ding et al. (2017), Kimura et al. (2014) for rat; from Ayzenshtat et al. (2016), Dräger and Olsen (1981), Garrett et al. (2014), Van Hooser et al. (2005), Ross and Kay (2004), Bock et al. (2011), Goltstein et al. (2013), Moeyaert et al. (2018), Muir and Kampa (2015), Palagina et al. (2017), Wang et al. (2006), Yoshida et al. (2012) for mouse. The details are summarized in Table 1.

METHOD DETAILS

Analysis of anatomical data

The V1 (A_V) and retina (A_R) sizes, and the number of RGCs (N_R), were obtained from the references above. The number of V1 neurons (N_V) in a two-dimensional (2-D) section of V1 was estimated by multiplying the V1 area size by the 2-D surface density of V1 neurons. The surface density was estimated from the two-photon imaging data of each species (Figure S4), which was observed to be fairly consistent across species (within −11.3 to +9.1% of average) except in macaques (1.50 times higher). This estimation well matched the previous observation that the surface density of V1 neurons is consistent across mice, rats and cats, but 2.5 times higher in macaques (Srinivasan et al., 2015).

For precise estimation of retino-cortical mapping across retinal space, both physical cell density and the magnification factor between two areas are required, but this information for all species across eccentricity is currently not available. Instead, we assumed that the mapping ratio is quasi-constant across eccentricity based on the cat and monkey data (Figure S2). Then, we estimated the retino-cortical mapping ratio (Φ = number of V1 neurons per RGC) by dividing the average number of V1 neurons by the number of RGCs (N_V/N_R).

Estimation of retino-cortical sampling ratio

The retino-cortical sampling ratio (Γ) of each species was obtained by dividing the nearest-neighbor pinwheel distance in the underlying retinal structure (d_{PW}) by the distance between neighboring V1 neurons (d_{V1}), as follows:

$$\Gamma = \frac{d_{PW}}{d_{V1}} = \frac{\Psi S d_{ON/OFF}}{d_{V1}} = \Psi S \sqrt{\frac{N_V}{N_{ON/OFF}}} = \Psi S \sqrt{\frac{N_V}{0.5 N_R}} = 0.76 S \sqrt{\Phi}$$

Here $d_{ON/OFF}$ represents the expected average lattice distance of ON/OFF RGC mosaics, S represents the spatial period of the orientation map estimated in RGC mosaics (normalized by $d_{ON/OFF}$; Figure S1C), Ψ represents the observed distance between the nearest neighboring pinwheels normalized by the map period in cat V1 (= 0.534; estimated from Figure 3 of Müller et al. (2000) and $N_{ON/OFF}$ represents the average number of ON/OFF RGCs in the entire retina, which was assumed to be half of the whole number of RGCs (N_R).

For the cats, macaques and mice, we applied the spatial period of the orientation map (S) estimated from the RGC mosaics data obtained from each species (cat, 3.86, [Zhan and Troy, 2000]; mouse, 4.59, [Bleckert et al., 2014]; macaque, 5.17, [Vidne et al., 2012]) as follows:

$$S = \frac{1}{SF_{FFT}} \times \frac{1}{d_{ON/OFF}}$$

where SF_{FFT} is the spatial frequency of orientation tuning. To determine the spatial frequency of orientation tuning, the local orientation tuning was estimated at each retinal location, after which the resulting organization was smoothed by 2D Gaussian filters of different sizes (Figure S1B). To find a consistent spatial period, the peak frequency calculated from an FFT analysis of maps was measured for various filter sizes, and the spatial frequency at a stable plateau was selected (Figure S1C). For the five other species, the RGC mosaic data were not currently available. Accordingly, the size of the retinal cluster was assumed to be the average of three representative values obtained from cats, monkeys and mice (4.54).

Connectivity and receptive field models

To model a V1 receptive field, we assumed that the RGCs are statistically wired to local V1 neurons around the corresponding cortical location (Ringach, 2007). The connection weight (w) of the retino-cortical projection was constrained by a 2D Gaussian distribution with a standard deviation (σ_{con}) of $0.4 d_{OFF} = 41$ μm in the retinal space such that a couple of ON and OFF RGCs strongly contributed to the formation of the receptive field of a V1 neuron (Ringach, 2007), where d_{OFF} is the average lattice distance between OFF RGCs (0.102 mm).

We assumed that parameters for the retino-cortical projection could be approximated as quasi-constant in the local eccentric area. In particular, we assumed that every cortical cell receives input from a similar number for RGCs regardless of variation in RGCs density and retino-cortical magnification, because the density of the RGCs and retino-cortical magnification are proportional across retinal eccentricity in the observed RGC data at large scale (Chaplin et al., 2013; Wässle et al., 1990) (Figure S2). Synaptic weighting between i^{th} RGC and j^{th} cortical sites (w_{ij}) was defined as

$$w_{ij} = \frac{1}{\sigma_{con}\sqrt{2\pi}} exp\left(-\frac{d_{ij}^2}{2\sigma_{con}^2}\right)$$

where d_{ij} represents the distance from the center of the ith RGC to the projected location of the jth cortical site.

The receptive fields of RGCs were defined as a center-surround 2D Gaussian model. The standard deviation of the surrounding region was set to three times that of the center region (Croner and Kaplan, 1995). The receptive field of the ith RGC ($\Psi_{i,\,RGC}$) was defined as

$$\Psi_{i,\,RGC} = \pm\left(\frac{1}{\sigma_{RGC}\sqrt{2\pi}}\exp\left(-\frac{r_i^2}{2\sigma_{RGC}^2}\right) - \frac{1}{3\sigma_{RGC}\sqrt{2\pi}}\exp\left(-\frac{r_i^2}{18\sigma_{RGC}^2}\right)\right)(+ : ON\ cell,\ - : OFF\ cell)$$

Here, r_i is the distance vector from the center of the ith RGC to each position of the visual field. Additionally, σ_{RGC} was set to 43.1 μm for ON and 38.4 μm for OFF RGC based on the two-sigma rule stating that the sigma of the RGC receptive field is around half of the cell-to-cell distance (Balasubramanian and Sterling, 2009). The receptive fields of V1 neurons were defined by the linear sum of the receptive fields of connected RGCs, so the receptive field of jth cortical site ($\Psi_{j,\,V1}$) was defined as

$$\Psi_{j,\,V1} = \sum_i w_{ij} \cdot \Psi_i^{RGC}$$

All simulations were performed using MATLAB 2017a.

Measurement of cortical functional tuning

The preferred orientation and selectivity of the calculated V1 receptive field was estimated from its Fourier transform $\Psi(\omega)$. The preferred orientation (θ_{Pref}) and preferred spatial frequency (ω_{pref}) were defined as $\theta_{Pref} = \arg(\mu)/2$ and $\omega_{pref} = |\mu|$, where

$$\mu = \int |\Psi(\omega)||\omega| \exp(2i\,\arg(\omega)) d\omega \Big/ \int |\Psi(\omega)| d\omega$$

The orientation selectivity index (OSI) was defined as

$$OSI = \left| \int |\Psi(\omega_{pref}, \theta)| \exp(2i\theta) d\theta \right| \Big/ \int \left|\Psi(\omega_{pref}, \theta)\right| d\theta$$

The tuning similarity between two cortical neurons was obtained by measuring a Pearson correlation coefficient of their receptive field in the frequency domain (Figure 2E). The tuning similarity was measured from all the pairs of cortical neurons and was averaged over distance. Receptive fields were Fourier transformed (FFT) and the non-linear response of neurons, R_f, was estimated by applying a sigmoidal kernel,

$$R_f = 1/\left(1 + e^{40(\Psi(\omega)-0.15)}\right)$$

To examine the effect of an instance of cortical nonlinearity on the organization of orientation tuning (Figure S3A), the responses of model V1 neurons with a nonlinear response function were simulated by determining the response to a grating input. A classical linear-nonlinear model for the cortical response was applied to mimic the spike firing rate of V1 neurons (Paninski et al., 2007). First, for a grating stimulus (G), the cortical input for j^{th} cortical cite ($I_{j,V1}$) was obtained from the weighted sum of the multiplication between the receptive field of the ith RGC ($\Psi_{i,\,RGC}$) and the grating stimulus as follows:

$$I_{j,V1}(G) = \sum_i w_{ij} \cdot \Psi_{i,\,RGC} \cdot G$$

where the drifting grating was designed as a sine function of twenty different spatial frequencies (0.5–8 cycle/degree).

The cortical input was then provided to a nonlinear response function modeled as a sigmoidal function, resulting in the response of V1 neurons, $R_{j,V1}$ as follows:

$$R_{j,\,V1}(G) = \left(1 + exp\left(-\frac{I_{j,V1}(G) - 0.15}{0.025}\right)\right)^{-1}$$

The preferred orientation was defined as the orientation of the stimulus that generates the largest response. All simulations were performed using MATLAB 2017a.

QUANTIFICATION AND STATISTICAL ANALYSIS

Two-sample Kolmogorov-Smirnov test was used to determine the significance of spatial clustering of cortical orientation tuning (Figure 2), Φ = 2.7 versus 0.33 (blue versus red), *p = 6.0×10^{-4}; Φ = 0.30 versus 0.33 (green versus red), p = 0.43; Φ = 0.30 versus shuffled (green versus black), *p = 2.1×10^{-2}, Φ = 2.7, n = 5.66×10^{6}; Φ = 0.33, n = 8.27×10^{4}; Φ = 0.3, n = 6.82×10^{4} pairs from 100 repeated simulations; (Figure 2E), Data versus Φ = 0.09 as estimated for mice (black versus dark red), p = 0.23). The F-test was used to determine the significance of the fitted slope in Figure S2C (p = 0.85, n = 28) and S2F (p = 0.12, n = 11). The Wilcoxon rank-sum test was used to determine the significance of difference between the spatial clustering of cortical orientation tuning in gray squirrels and in tree shrews (Figure S3F, *p = 0.017, n = 4000). The one-way ANOVA was used to determine the significance of difference in the cell-to-cell distance and cell density across the species except the monkey (Figure S4B, *p = 1.2×10^{-4}; Figure S4C, *p = 6.7×10^{-4}, n = 28). The Wilcoxon rank-sum test was used to determine the significance of difference in the cell-to-cell distance and cell density between the monkey and the average of other species (Figure S4B, p = 0.82; Figure S4C, p = 0.87, n = 37). Shaded areas or error bars indicate the standard deviation in Figures 2D, 3C, S1C, S1D, S1F, S3B, S3D, S3I, S4B, and S4C.

DATA AND CODE AVAILABILITY

Data and code used in this study are available from the Lead Contact upon request.